Presented at the 29th European PV Solar Energy Conference and Exhibition, 22-26 September 2014, Amsterdam, The Netherlands

FAST HOT SPOT EVALUATION

Ino Geisemeyer, Fabian Fertig, Wilhelm Warta, Stefan Rein, Martin C. Schubert
Fraunhofer Institute for Solar Energy Systems
Heidenhofstr. 2, 79110 Freiburg, Germany
Phone: +49 (0) 761 4588 5661, email: ino.geisemeyer@ise.fhg.de

ABSTRACT: We present a method which provides simple and fast evaluation of the hot spot potential of solar cells before the module assembly process. The method is based on convoluting power dissipation images measured with infrared thermography with specially designed point spread functions. The result is a temperature image of a cell under critical shading conditions of the module. For validation of the method we conduct a laboratory experiment with bare cells. Measured temperature fields of exemplary solar cells are compared to simulated images. The transfer from laboratory conditions for bare cells to outdoor module conditions is performed by using additional three-dimensional numerical simulations. It is shown that the method can in principle be used for inline application.
Keywords: PV Module, Shading, Shunts, Qualification and Testing

1 INTRODUCTION

Evaluating the hot spot risk of a solar cell prior to module fabrication is a demanding task. Of various methods three approaches are prominent: 1) To evaluate the cells' global reverse characteristics, 2) to evaluate ordinary thermography images taken after few milliseconds with the cells being reverse-biased and 3) to use spatially resolved lock-in thermography (LIT) and numerically simulate steady state temperature fields in the module for each cell with the boundary conditions of worst case shading.

Assessing the hot spot risk of a solar cell by evaluating the global reverse bias characteristic is an incomprehensive approach since the characteristic can be caused by local shunting as well as local process- or material-induced breakdown [1] with strongly varying influence on the global reverse characteristic. The actual power dissipation density can cause irreversible damage to the module [2] without being considered as critical.

Assessing instead the hot spot risk by evaluating an infrared image of a cell reverse-biased for a short time is often based on statistics between short-time and long-time maximum temperatures. It has been shown that the correlation tends to be linear but has a broad distribution making it difficult to define threshold criteria [3, 4], consequently leading to overestimation of the risk of a large number of cells for a conservative criterion and otherwise to underestimation of the risk of individual cells.

The third approach is based on power-calibrated images measured with LIT [5]. This measurement technique makes use of short excitation times and a lock-in algorithm to increase the signal to noise ratio compared to standard thermography of excited sources. With the resulting power-calibrated images steady state temperature fields can be simulated for cells built into modules under critical shading conditions [6, 7].

Up to now the last approach is the most promising of the three because it implements the local behaviour of ohmic shunting as well as process- and material-induced reverse breakdown with the highest accuracy. However, two problems have thus far prevented a straightforward application of the method: while lock-in thermography images can generally be taken in 10 ms [8], the numerical simulation requires computational time of approximately 10 min. And although the simulation predicts significantly higher temperatures for certain isolated hot spots at the cell surface than at the module backsheet [6], this could not yet be proven in typical module experiments. There, temperatures are normally measured at the module's backsheet.

We present a method which provides significantly simpler and faster evaluation of the hot spot potential by avoiding the three-dimensional thermal numerical simulation. The approach is to convolute power dissipation images measured with infrared thermography with specially designed point spread functions. This step without significant loss of information lets inline applicability come within reach and is a further improvement to a fast temperature prediction at the backsheet presented in [9]. A new iterative approach implements the nonlinearity of the heat diffusion problem to enable temperature prediction with sufficient accuracy. The computation can be carried out in less than one second. The results are verified in a laboratory experiment which enables to measure the temperature directly on the solar cell surface.

2 EXPERIMENTAL STEPS

First, a laboratory experiment is carried out to measure the solar cell temperature directly on the cell's surface for conditions approximating hot spot heating in modules. The electrical conditions are determined via a network simulation.

Secondly, the proposed inline-feasible simulation is carried out for the same conditions as in the laboratory experiment and compared to the experimental results. Special emphasis is put on the requirements to the power-calibrated input images measured with infrared imaging.
Finally, worst case scenarios are examined theoretically for uncertainties in temperature prediction based on the used measurement technique for power-calibrated images.

2.1 Experimental steady state temperatures

Since the cell temperature during typical module hot spot tests cannot be measured directly at the cell surface we conduct an experiment without encapsulation. The bare cell is placed horizontally between contacting strips, so that most of the cell area is in direct contact with air. A reverse voltage is applied continuously and the cell temperature in thermal equilibrium measured with an infrared camera. This temperature image serves as benchmark for our proposed simulation of steady state temperatures.

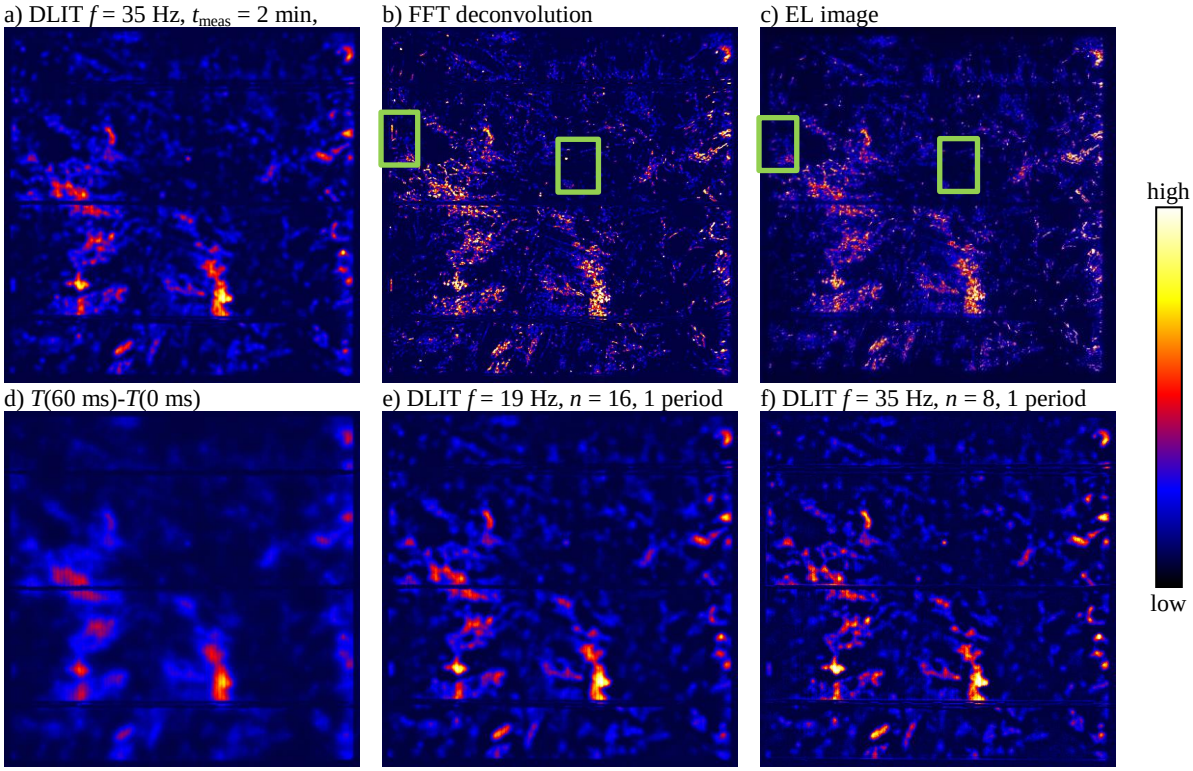

Figure 1: Power-calibrated images with differing blurring and noise. The parameter n denotes the number of images per lock-in period with frequency f and t_{meas} the total measurement time. The power-calibrated images serve as input for the inline-feasible simulation of the steady state temperature field in critical shading conditions. Image b), computed from image a) with fast fourier transformation (FFT), has the highest accuracy in power density and serves as reference to the other input images. The electroluminescence (EL) image cannot be calibrated to power dissipation by fundamental reasons.

2.2 Critical operating points

The power density leading to a temperature increase in a partially shaded cell in a module can be divided into two main parts: one due to photo-generated current passing the junction and one due to individual reverse current through shunting or junction breakdown. These parts depend on the reverse-biasing of the cell, hence the operating point, which can be extracted from an electrical network simulation [2] as a function of the shading ratio. On the one hand for these operating points the steady state temperatures according to section 2.1 are measured and on the other hand for these operating points the input images for the simulation are generated.

2.3 Infrared imaging

The temperature increase due to individual reverse currents through shunting and junction breakdown can be measured quantitatively and spatially resolved with infrared imaging and calibrated to dissipated power. It can reveal ohmic shunts with linear *current-voltage* characteristics as well as process- and material-induced local reverse junction breakdown which have been intensively studied [1]. By using infrared imaging with simultaneous illumination of the cell the interaction with the photo-generated current can be determined, but in most cases it is sufficient to assume independent superposition as will be done in the following.

The proposed method to simulate temperature fields by convolution of infrared images depends crucially on how good the infrared images reflect the actual power density. Since infrared cameras have a finite resolution, the ideally measured power density would be correct up to one pixel. However, sufficient signal to noise ratios can usually only be reached after a certain integration time, hence, also excitation time of the cell, during which thermal diffusion leads to blurring. The elementary two-dimensional temperature field when caused by a point unit power source is called the point spread function of the imaging system. Based on specially designed point spread functions and common image calibration techniques, in the following, power density imaging for possible inline application is derived and discussed regarding the accuracy of the obtained power density.

2.4 Lock-in thermography (LIT)

Due to thermal diffusion during image acquisition the thermal signal of a single point power source is laterally spread over a region which depends on the lock-in frequency. More precise, the temperature field can be described by a Kelvin function of the distance to the source divided by the thermal diffusion length as explained in detail in [5]. For a typical offline measurement setup with lock-in frequency of 35 Hz this region is about 16 mm^2, hence the image appears blurred. This is illustrated in Fig. 1a for a multi-crystalline 6-inch solar cell measured in the dark (DLIT) with periodically repeated excitation for a total measurement time of 2 min. The MWIR camera with MCT-FPA detector used has an active resolution of 512 x 512 pixels which leads to a pixel length of 0.3 mm when imaging the total area of a 6-inch solar cell. Hence, the thermal blurring extends over several pixels. Using the proportionality method [5]

for calibration to power density, which means that each pixel is divided by the image mean and multiplied by the measured dissipated power, therefore distributes the actual power of a unit point power source to a Kelvin function over several pixels.

However, if the signal to noise ratio is sufficiently high the image can be deconvoluted to display the power density up to an accuracy of one pixel. The result of such image processing with fast complex Fourier transformation [5] is shown in Fig. 1b. For comparison an electroluminescence image of the reverse-biased cell (ReBEL) is shown in Fig. 1c which does not suffer from thermal diffusion but cannot be calibrated to power dissipation by fundamental reasons [10] and therefore is not suited for temperature prediction. Furthermore, ohmic shunts as marked with the green boxes are not visible in ReBEL-images.

The high quality (Fig. 1a) and high resolution (Fig. 1b) images serve as benchmarks for inline applicable imaging.

2.5 Alternative infrared imaging methods

One could attempt to reduce the lock-in algorithm to just two images, one at the start of heat supply and one at the end of heat supply, to reduce the requirements on the speed of the imaging system. In the following, the consequences of integration time and, hence, thermal diffusion for the accuracy of the proposed method will be discussed without consideration of noise.

A power-calibrated thermography image after 60 ms is shown in Fig. 1d. The calibration is done according to

$$P_{xy} = \frac{T_{xy}(60ms) - T_{xy}(0)}{\langle T_{xy}(60ms) - T_{xy}(0)\rangle} \frac{P_{\mathrm{in}}}{L^2} \qquad (1)$$

where the index *xy* indicates the pixel position, P_{in} is the measured dissipated power, L the pixel length and < > indicates an arithmetic average over all pixels of the image.

For comparison, Fig. 1e and 1f show power-calibrated LIT images taken with just one lock-in period for two different frequencies and images per period. All power-calibrated images have the same scaling to enable direct comparison. Although the mean power of all calibrated images is equal, they differ in spatial resolution caused by thermal diffusion and signal to noise ratio depending on the used imaging technique.

3 DEVELOPMENT OF THE POINT SPREAD FUNCTIONS (PSF)

3.1 Short-time heat supply

For the case of common infrared imaging the temperature field after a few milliseconds can be constructed using the PSF of a continuous vertical line source [11]

$$T(r,t) = -\frac{Q}{4\pi K} Ei\left(-\frac{r^2}{4\kappa t}\right) + T_0, \qquad (2)$$

where r is the radial distance from the line source and T_0 the temperature at the start of constant heat supply Q in units power per length. The abbreviation Ei represents the exponential integral function and K and κ are the material parameters thermal conductivity and diffusivity, respectively. Due to the assumption of a point power source, the temperature signal in the source origin tends to infinity. This non-physical behaviour can be overcome

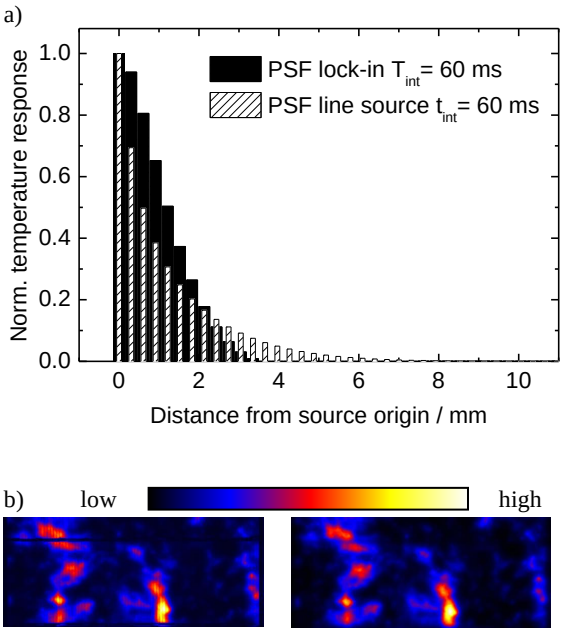

Figure 2: a) Normalized temperature response to a continuous line source after 60 ms and to a point source with lock-in period of 60 ms. Intensities are adjusted to the finite resolution of the imaging system. b) Detail of the infrared image corresponding to Fig. 1d and simulated temperature image by convolution of Fig. 1b.

by integrating the temperature response signal over the pixel area under investigation, thereby simulating the working principle of the infrared camera. For simplification, this procedure is done for the pixel describing the response in source origin, whereas the temperature response for all other pixels $(x, y) \neq (0,0)$ is approximated by the temperature in the centre of each pixel

$$\mathrm{PSF}_{xy}(t) = T(D\sqrt{x^2 + y^2}, t)\,, \qquad (3)$$

where D is the pixel length. This approach is similar to the construction of PSFs for LIT signals as described in [5] and applied in section 2.

The resulting temperature response after t_{int} = 60 ms is shown in Fig. 2a for radial direction. The signal is more blurred than the temperature response of LIT with a lock-in period of T_{int} = 60 ms which is shown in the same diagram. To measure 90% of the signal the integration area must extend over a radius of more than 5 mm.

For the convolution of power-calibrated images with PSFs we use the algorithm proposed in [5] which implements mirror sources to account for the back-reflection of heat waves.

A detail of the simulated temperature after 60 ms by convoluting the Fourier-transformed and power-calibrated LIT image Fig. 1b is shown in Fig. 2b together with the measured infrared image. Good agreement can be reached. However, due to the large diffusion length and typical experimental noise, the reverse operation deconvolution for power density construction is difficult. Single thermography images of this kind therefore carry less information about localised power sources.

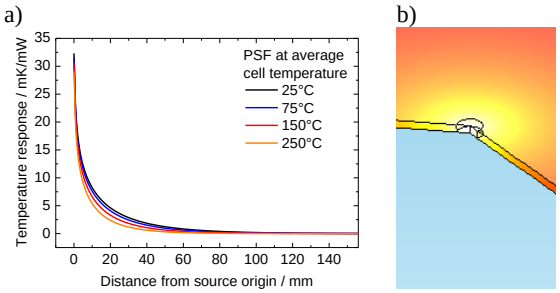

Figure 3: a) PSF of a unit power source at exemplary cell temperatures. b) Schematic of the axisymmetric finite element simulation.

3.2 Long-time heat supply

Generally, the approach of convoluting images of point power sources with point spread functions of temperature distributions necessitates a linear heat diffusion problem. This is approximately given for heat supply for a few milliseconds since the resulting temperature differences to the environment are small. Hence, no significant heat transfer to the environment is established. In this case the cell surface can be treated as thermally insulating. However, for ongoing heat supply the temperature difference and therefore the heat transfer to the environment increases until an equilibrium state is reached. This can be described by nonlinear boundary conditions with the heat flux

$$\dot{q} = h(T_{\text{cell}}, T_{\text{env}}) \cdot (T_{\text{cell}} - T_{\text{env}}), \qquad (4)$$

where T_{cell} is the cell temperature and T_{env} the temperature of the environment not influenced by the cell. The total heat transfer coefficient h includes radiation and convection. The heat diffusion equation can be linearized by determining h at all temperature differences $T_{\text{cell}} - T_{\text{env}}$ and using an iterative approach to determine the temperature difference.

First, the point spread functions are computed using a numerical 2-D axisymmetric finite element simulation. The simulation domain comprises a solar cell stretched so far as necessary to approximate open boundaries. Radiation and convection coefficients can be determined from experiments or additional simulations. A unit power source is implemented into the centre volume having the height of the solar cell and surface area of one pixel. An additional homogeneous power source is implemented to cause the average temperature difference between cell and environment. The unit power source has to be chosen so small that the additionally caused temperature response does not change the heat transfer coefficient significantly. The temperature signals are extracted according to paragraph 3.1 with averaging over the origin surface and centre values of all other pixels. Examples of the resulting point spread functions are shown in Fig. 3 together with a schematic of the power source volume.

The PSF to simulate the steady state temperature is chosen to be the PSF corresponding to the maximum temperature difference between cell and environment. This can be done in the following way: First a PSF corresponding to a guessed temperature difference is used for convoluting a power-calibrated image. Then, the maximum resulting temperature is determined and the PSF corresponding to this temperature is used for a second convolution of the initial power-calibrated image.

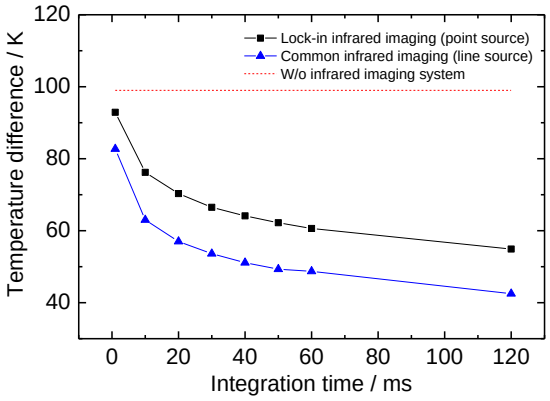

Figure 4: Simulated maximum temperatures for a power source of $P_{\text{in}} = 2.7$ W concentrated in one pixel. The dotted line reflects direct simulation without blurring of imaging systems, the black curve implements blurring due to the lock-in imaging procedure and the blue due to imaging of relative heating.

This process is carried out until no significant change in maximum temperature occurs. Usually, three iterations are sufficient.

By applying just one PSF to the whole image, the influence of sources leading to temperatures colder than in the maximum temperature region is underestimated. However, as will be shown in section 5, the prediction of maximum temperature is sufficiently good.

4 SENSITIVITY ANALYSIS

In this section the requirements to the power density images as basis for the convolution procedure are studied. The approach is the following: A certain chosen power density is convoluted to result in the temperature signal the imaging setup would detect. Then the signal is calibrated to a power density and finally convoluted with the PSF of the long-time heat supply to result in steady state temperatures. This image is compared to the direct convolution of the initial power density to steady state temperatures leaving out the blurring caused by the imaging techniques.

The successive convolution can alternatively be carried out in Fourier-space, reducing the operation to a simple matrix multiplication.

Since the current at reverse voltage can be of point-like form, e.g. ohmic shunting, or of more distributed form as for defect-induced breakdown in mc-Si cells, different geometries are studied.

As follows by the calibration procedures described in paragraph 2.4 and by eq. (1), a source distributed homogeneously over the whole cell area leads to the same maximum temperature regardless which imaging system is used. This is also true if the source area is significantly larger than the thermal diffusion length corresponding to the imaging setup, cf. Fig 3a. Deviations of the temperature can be expected if the source area is comparable to the thermal diffusion length. The worst case is a power density being zero everywhere except in one pixel. Since the iterative approach of convolution described in section 3.2 implements the non-linearity of the heat diffusion equation, the worst case

Table I: Maximum simulated temperature difference by using different power-calibrated infrared images according to Fig. 1.

Fig. 1	a)	b)	d)	e)	f)
Max. ΔT / K	152.9	153.0	155.5	153.1	153.6

study cannot be performed in general for a unit power source in one pixel. For an example study of the accuracy of the temperature prediction the single pixel power source is set to P_{in} = 2.7 W. This choice resembles an actual measurement further examined in section 5. The numerical finite element simulation for a 6-inch cell results for this power density in a maximum temperature difference to the environment of ΔT_{max} = 95.7 K. Directly using the convolution procedure on the initial power density yields a maximum temperature difference of ΔT_{max} = 99 K. This is the reference for the study of input data with variation of image integration time in the case for infrared imaging of relative heating with two images and lock-in period in the case for LIT, respectively. The difference in simulated maximum temperature is probably caused by the circumstance that for the finite element simulation of the complete cell a cubic volume instead of a cylindrical is used. The maximum temperatures when integrating the blurring by the imaging system are shown in Fig. 5. At integration time of 60 ms underestimation of the maximum temperature of 50% with the imaging technique for relative heating and 40% with the lock-in imaging technique is possible.

Please note, that this study does not include electrical properties such as, e.g. spreading resistance, which can lead to a limitation of the possible power density [6].

5 APPLICATION TO EXEMPLARY CELLS

First, the convolution is applied to all power-calibrated images of Fig. 1 and the resulting maximum temperature differences to the environment shown in Table 1. All simulated temperatures agree within 3 K, therefore, the resulting temperature is not underestimated by using images with more blurring as input. However, since the hottest spot is stretched over more than several thermal diffusion lengths, which is given by the setup of the imaging system, this result agrees well with the expectations. Furthermore, the highest power density is comparably low with P = 24 mW/pixel.

In Fig. 5 the steady state temperature simulation results for three cells at different reverse bias conditions are compared. The first column shows simulated temperatures gained with the finite element approach, which is the offline approach. The second column shows results of the inline convolution approach with power-calibrated images measured with LIT at a lock-in frequency of $f_{lock\text{-}in}$ = 35 Hz, hence a period of 28 ms. The third column gives the results of using the temperature difference image after 60 ms of power supply. The last column shows directly measured infrared images.

The first three rows show good agreement between the inline simulation and the temperature measurements. Hence, it is also negligible if power-calibrated lock-in infrared images or the power-calibrated images of relative heating after 60 ms are used as input for the

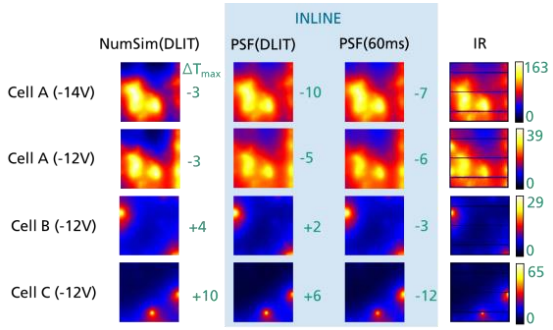

Figure 5: Simulated and measured steady state temperatures difference between hottest spot and environment for reversed bias cells contacted horizontally in air. NumSim denotes the offline approach using finite-element simulation, PSF denotes the inline-feasible convolution approach and IR is for infrared images.

convolution procedure. This is again based on the fact, that the hottest spots extend over more than one thermal diffusion length and the maximum power per pixel is low. However, the last row shows an underestimation compared to the measured temperature for power images measured with the common infrared imaging system and an overestimation when using images measured with LIT. This spot turns out to be highly concentrated as can be seen in the steady state temperature images shown in Fig. 6. The totally dissipated power of this spot is 2.7 W, as was studied in the worst case analysis in section 3. Measuring this spot with low resolution as done in the first infrared image can underestimate the maximum temperature and makes the measurement dependent on

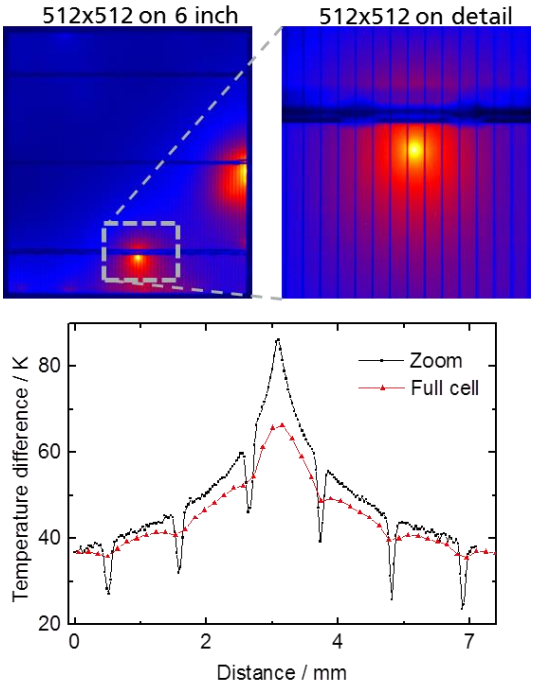

Figure 6: Temperature measurement with different resolution and line scan through the hottest pixel. Low resolution can lead to underestimation of maximum temperature differences.

the cell placement in respect to the camera. It turns out, that the actual hot spot temperature difference is above 85 K instead of 65 K. Therefore, the inline approach with the LIT image as input underestimates the actual temperature with more than 10 K, and using the power calibrated image of relative heating as input leads to underestimation of more than 30 K. This is caused by the different blurring of the calibrated images as described in section 4. For isolated hot spots with high power density, using LIT images with high frequency is preferable to reduce errors in predicting hot spot temperatures.

6 FURTHER STEPS IN ANALYSIS OF HOT SPOTS

The PSF are derived for cells contacted horizontally between contacting bars, so that most of the cell area is in contact with air. The transfer to module boundary conditions can easily be done by implementing the module boundary conditions in the axisymmetric finite element simulation and deriving new PSF. Thus, the individual design and materials of modules can be accounted for.

7 SUMMARY

We have presented a new method to predict hot spot temperatures of solar cells prior to module assembly based on convoluting power-calibrated images with point spread functions of temperature response. The convolution approach is inline-feasible and yields comparable results to offline simulation of steady state hot spot temperatures with finite element software. We have discussed the effects of infrared imaging techniques on power density determination and the resulting accuracy for steady state temperature predictions via the convolution approach.

ACKNOWLEDGMENT

This work has been supported by the German Federal Ministry of Economics under the frame of the “QUASSIM-PLUS” project (FKZ: 0325493A).

REFERENCES

[1] O. Breitenstein, J. Bauer, K. Bothe, W. Kwapil, D. Lausch, U. Rau, J. Schmidt, M. Schneemann, M. C. Schubert, J. M. Wagner, and W. Warta, "Understanding junction breakdown in multicrystalline solar cells," *Journal of Applied Physics*, vol. 109, p. 071101, Apr 1 2011.

[2] F. Fertig, S. Rein, M. Schubert, and W. Warta, "Impact of Junction Breakdown in Multi-Crystalline Silicon Solar Cells on Hot Spot Formation and Module Performance," presented at the 26th European Photovoltaic Solar Energy Conference and Exhibition, Hamburg, 2011.

[3] D. W. T. Roth, K. Meyer "Determining the Temperature of Bare Solar Cells and Local Hot Spots during IV Measurements," in *28th European Photovoltaic Solar Energy Conference and Exhibition*, Paris, 2013.

[4] T. Roth, R. Siebert, and K. Meyer, "From Short-term Hotspot Measurements to Long-term Module Reliability," *Energy Procedia*, vol. 55, pp. 504-508, 2014.

[5] O. Breitenstein, W. Warta, and M. Langenkamp, *Lock-in Thermography - Basics and Use for Evaluating Electronic Devices and Materials*, Second ed. Berlin/Heidelberg: Springer Verlag, 2010.

[6] I. Geisemeyer, F. Fertig, W. Warta, S. Rein, and M. C. Schubert, "Prediction of silicon PV module temperature for hot spots and worst case partial shading situations using spatially resolved lock-in thermography," *Solar Energy Materials and Solar Cells*, vol. 120, Part A, pp. 259-269, 2014.

[7] I. Geisemeyer, F. Fertig, W. Warta, S. Rein, and M. C. Schubert, "Impact of reverse breakdown in shaded silicon solar cells on module level: simulation and experiment," in *Proceeding of the 27th European Photovoltaic Solar Energy Conference, Frankfurt, Germany*, 2012.

[8] M. Kasemann, W. Kwapil, M. C. Schubert, H. Habenicht, B. Walter, M. The, S. Kontermann, S. Rein, O. Breitenstein, J. Bauer, A. Lotnyk, B. Michl, H. Nagel, A. Schütt, J. Carstensen, H. Föll, T. Trupke, Y. Augarten, H. Kampwerth, R. A. Bardos, S. Pingel, J. Berghold, W. Warta, and S. W. Glunz, "Spatially resolved silicon solar cell characterization using infrared imaging methods," in *Proceedings of the 33rd IEEE Photovoltaic Specialists Conference*, San Diego, USA, 2008.

[9] F. Fertig, I. Geisemeyer, H. Lindner, M. Demant, M. C. Schubert, S. Rein, "Cell-induced Hot Spots in Crystalline Silicon Solar Modules," in *PVSEC-23*, Taipei, 2013.

[10] O. Breitenstein, J. Bauer, K. Bothe, D. Hinken, J. Müller, W. Kwapil, M. C. Schubert, and W. Warta, "Can luminescence imaging replace lock-in thermography on solar cells?," *IEEE Journal of Photovoltaics* pp. 1-9, 2011.

[11] H. S. Carslaw and J. C. Jaeger, *Conduction of Heat in Solids*, second edition ed.: Clarendon Press, Oxford, 1959.